Fischer *et al.* **Supplementary Figure S1**

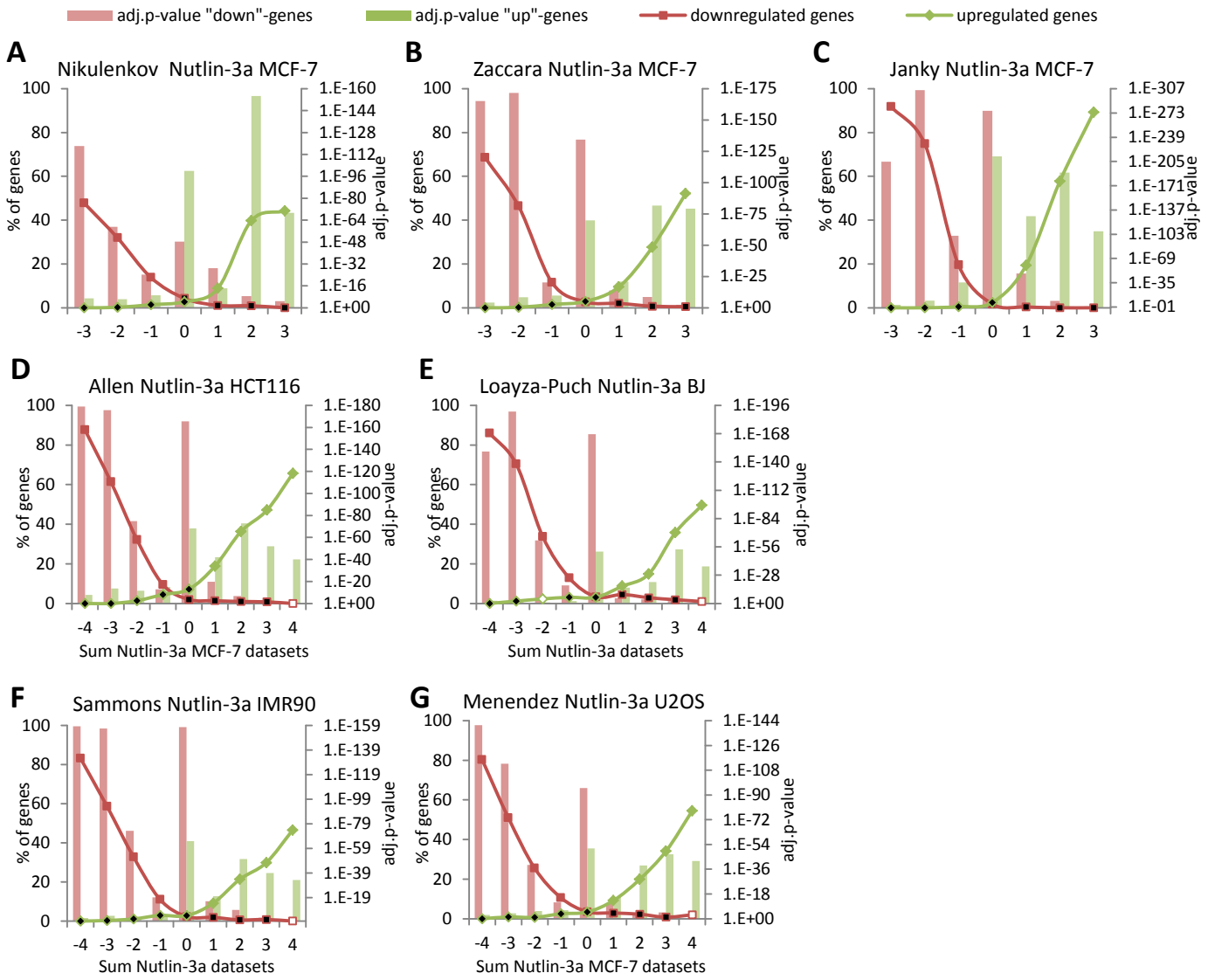

Supplementary Figure S1. Datasets of TP53-dependent gene regulation from Nutlin-3a treated ~~MCF-7~~ cells correlate strongly with each other. For each dataset of TP53-dependent gene regulation a gene can be found as upregulated "+1", downregulated "-1", or not regulated "0". The number of genes identified in **(A)** Nikulenkov et al ,**(B)** Zaccara et al., and **(C)** Janky et al. as either upregulated or downregulated is compared to the sum of the remaining three datasets from Nutlin-3a treated MCF-7 cells. The number of genes identified in **(D)** Allen et al., **(E)** Loayza-Puch et al., **(F)** Sammons et al. and **(G)** Menendez et al. compared to the sum of the four Nutlin-3a MCF-7 datasets. A two-sided Fisher's exact test was employed to test for significant over- and under-representation of gene sets and p-values were adjusted for multiple testing using Bonferroni correction. Colored and black data points are significantly over- and underrepresented, respectively (adj.p-value ≤ 0.05). White data points are not significantly different.

Fischer *et al.* **Supplementary Figure S2**

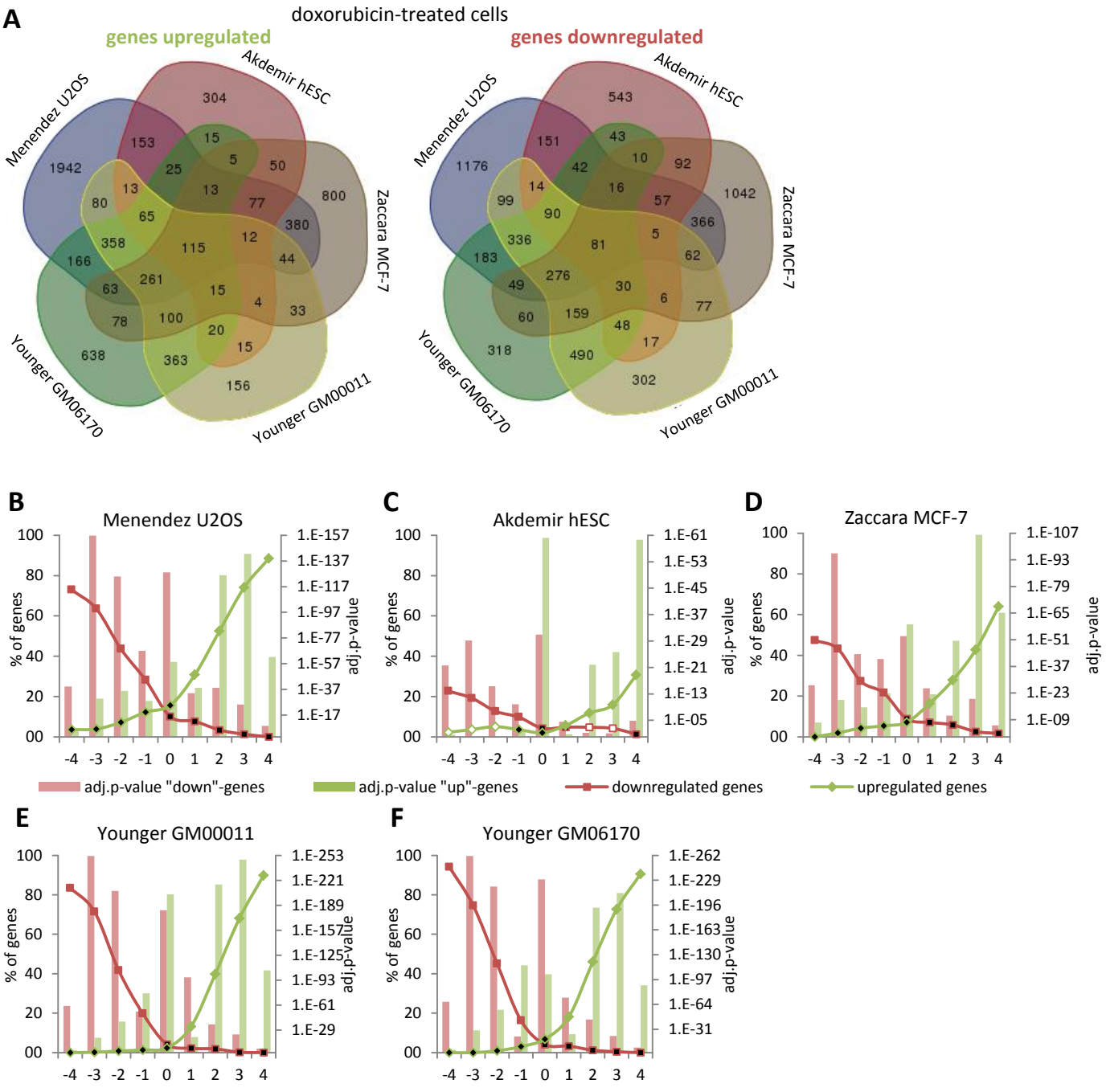

Supplementary Figure S2. Integration of expression profiling datasets of doxorubicin treated cells. (A) Venn diagram displaying the overlap of genes that were detected as being TP53-dependently up- or downregulated in the doxorubicin datasets from Menendez et al., Akdemir et al., Zaccara et al., and Younger et al. **(B)** The number of genes identified in (B) Menendez et al., **(C)** Akdemir et al., **(D)** Zaccara et al. and **(E and F)** Younger et al. as being TP53-dependently up- or downregulated is compared to the sum of the remaining four doxorubicin datasets. A two-sided Fisher's exact test was employed to test for significant over- and under-representation of gene sets and p-values were adjusted for multiple testing using Bonferroni correction. Colored and black data points are significantly over- and underrepresented, respectively (adj.p-value ≤ 0.05). White data points are not significantly different.

Fischer *et al.* **Supplementary Figure S3**

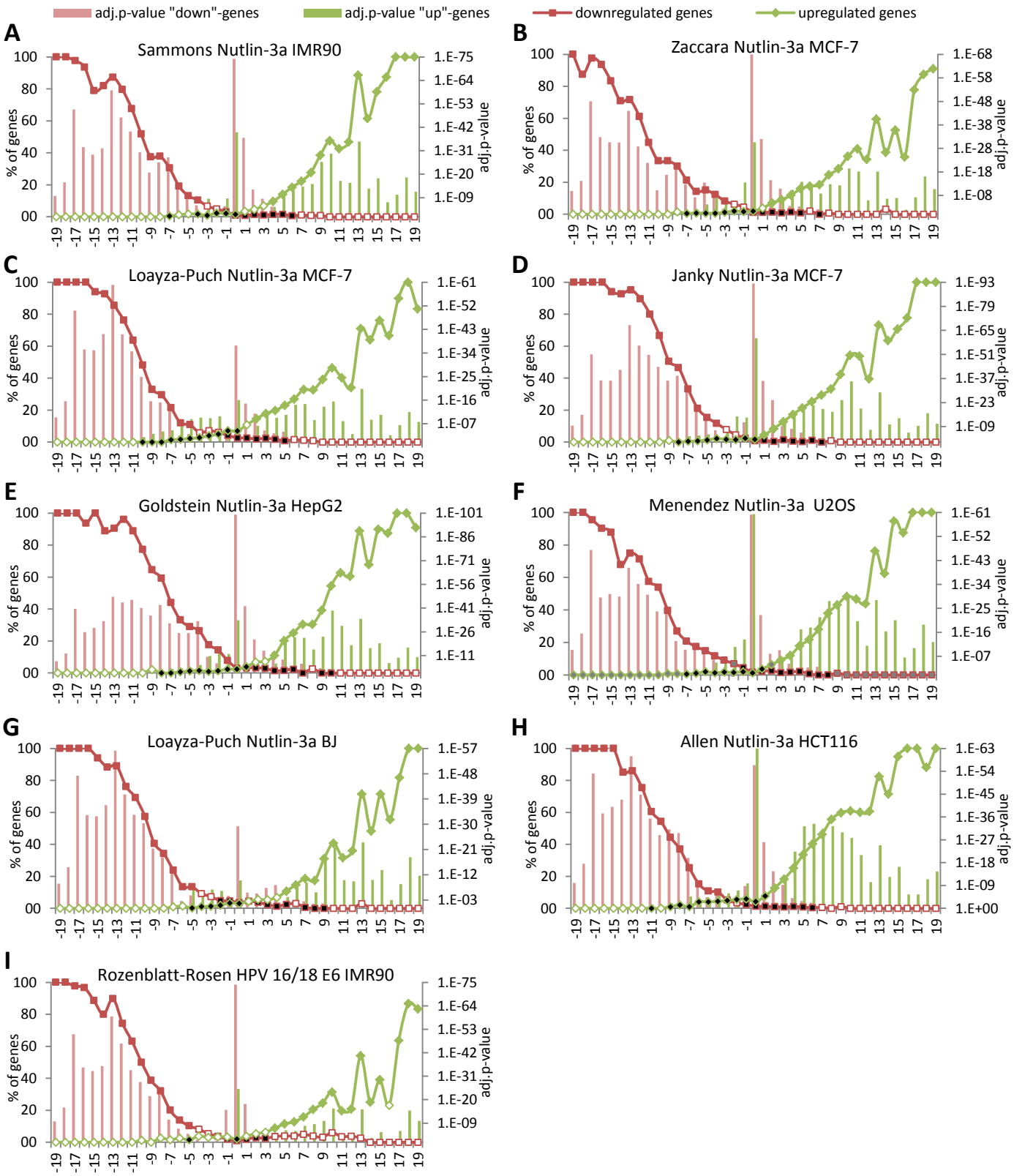

Supplementary Figure S3. Meta-analysis of TP53-dependent gene expression leads to a robust combined pan cell type and treatment dataset. In each dataset on TP53-dependent gene regulation a gene can be found as upregulated "+1", downregulated "-1", or not regulated "0". The number of genes identified in **(A)** Sammons et al., **(B)** Zaccara et al., **(C and G)** Loayza-Puch et al., **(D)** Janky et al., **(E)** Goldstein et al., **(F)** Menendez et al., **(H)** Allen et al. and **(I)** Rozenblatt-Rosen et al. datasets as either upregulated or downregulated by TP53 is compared to the sum of the remaining 19 datasets. A two-sided Fisher's exact test was employed to test for significant over- and under-representation of gene sets and p-values were adjusted for multiple testing using Bonferroni correction. Colored and black data points are significantly over- and underrepresented, respectively (adj.p-value ≤ 0.05). White data points are not significantly different.

Fischer *et al.* **Supplementary Figure S4**

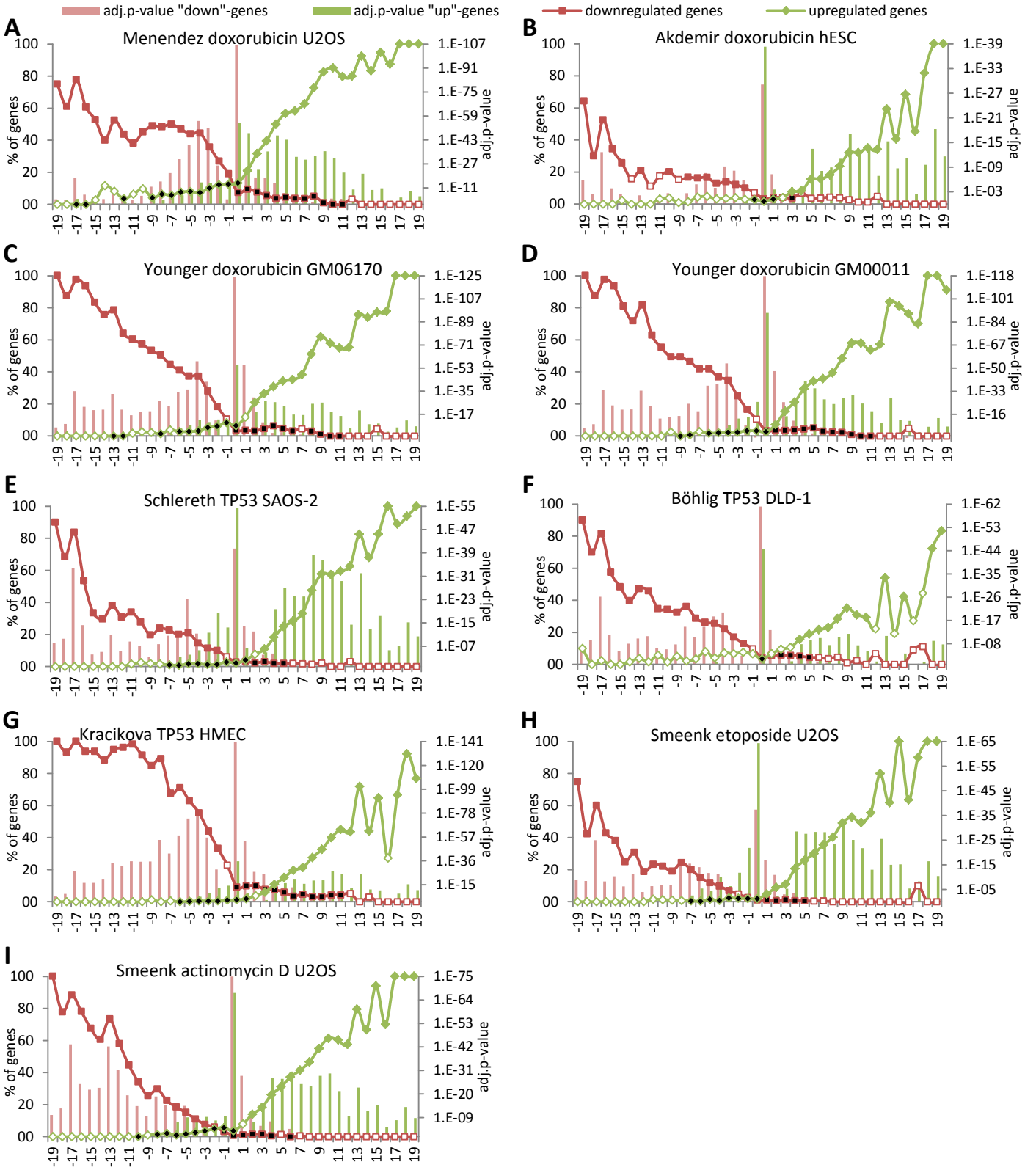

Supplementary Figure S4. Meta-analysis of TP53-dependent gene expression leads to a robust combined pan cell type and treatment dataset. In each dataset on TP53-dependent gene regulation a gene can be found as upregulated "+1", downregulated "-1", or not regulated "0". The number of genes identified in **(A)** Menendez et al., **(B)** Akdemir et al., **(C and D)** Younger et al., **(E)** Schlereth et al., **(F)** Böhlig et al., **(G)** Kracikova et al. and **(H and I)** Smeenk et al. datasets as either upregulated or downregulated by TP53 is compared to the sum of the remaining 19 datasets. A two-sided Fisher's exact test was employed to test for significant over- and under-representation of gene sets and p-values were adjusted for multiple testing using Bonferroni correction. Colored and black data points are significantly over- and underrepresented, respectively (adj.p-value ≤ 0.05). White data points are not significantly different.

Fischer *et al.* **Supplementary Figure S5**

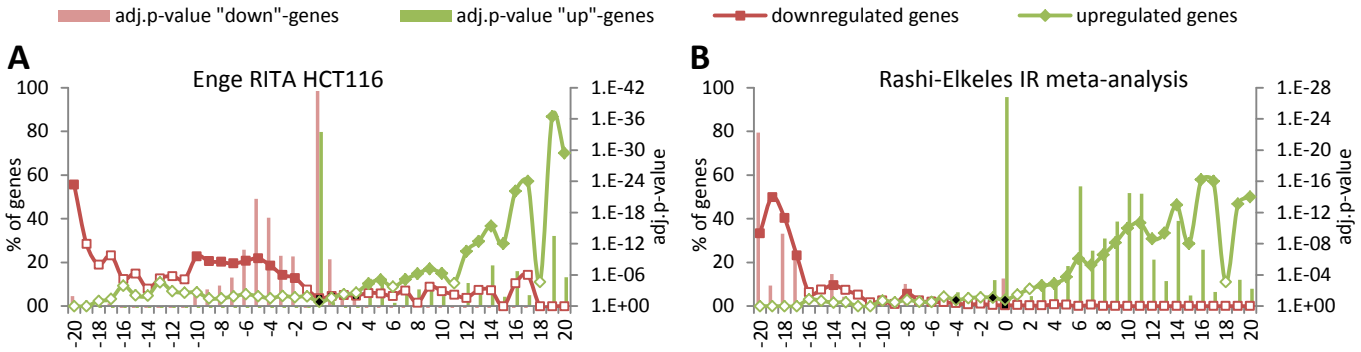

Supplementary Figure S5. RITA and ionizing radiation treatment yield distinct expression profiles. The number of genes identified in **(A)** Enge et al. and **(B)** Rashi-Elkeles et al. datasets as either upregulated or downregulated by TP53 is compared to the 41 *p53 Expression Score* groups. A two-sided Fisher's exact test was employed to test for significant over- and under-representation of gene sets and p-values were adjusted for multiple testing using Bonferroni correction. Colored and black data points are significantly over- and underrepresented, respectively (adj.p-value ≤ 0.05). White data points are not significantly different.

Fischer *et al.* **Supplementary Figure S6**

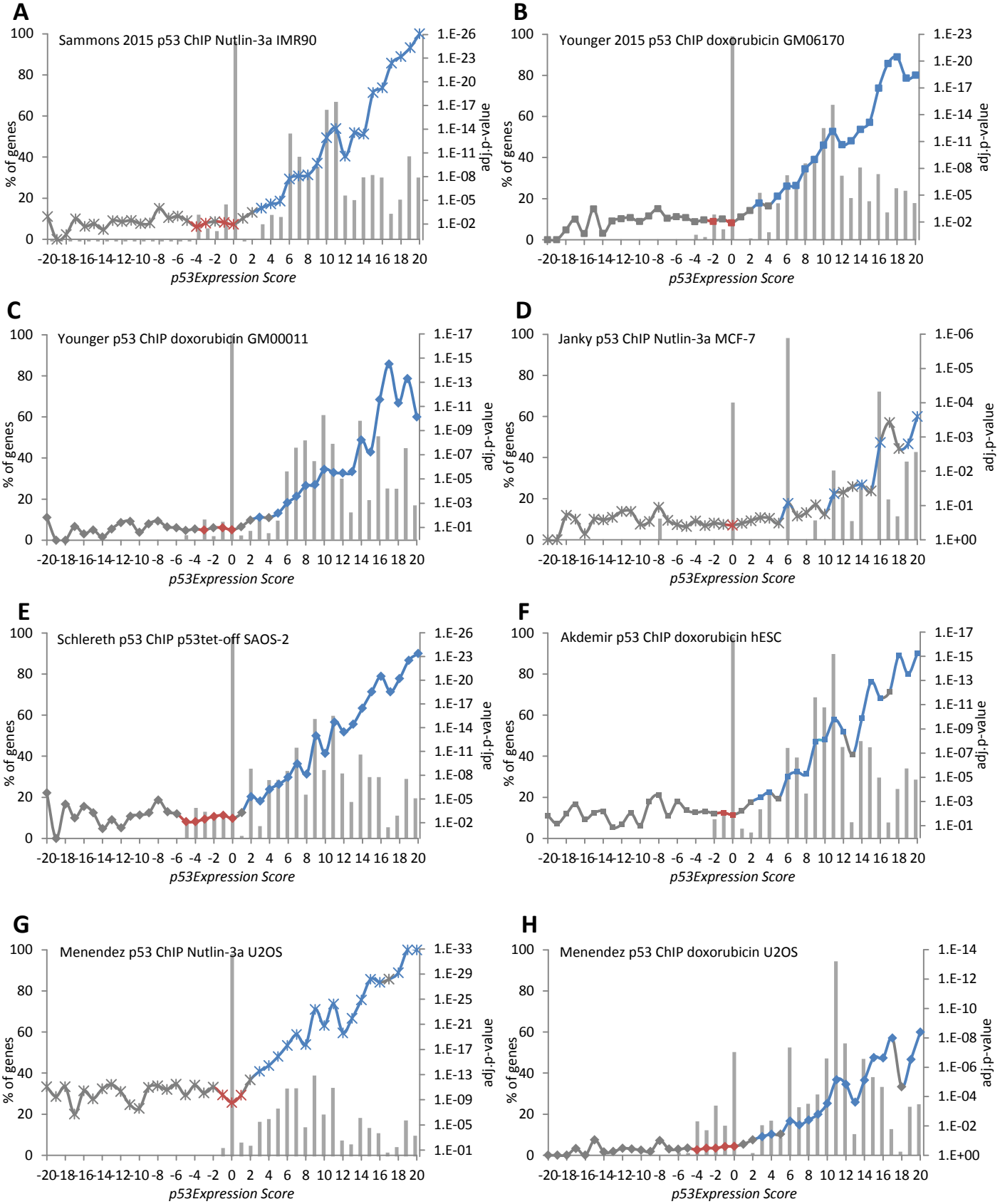

Supplementary Figure S6. TP53 chromatin binding associated with gene activation. The number genes found to be bound by TP53 within ±25 kb from their TSS across the 41 *p53 Expression Score* groups according to the datasets by **(A)** Sammons et al., **(B and C)** Younger et al., **(D)** Janky et al., **(E)** Schlereth et al., **(F)** Akdemir et al. and **(G and H)** Menendez et al.. Blue and red data points are significantly over- and underrepresented, respectively (adj.p-value ≤ 0.05). Grey data points are not significantly different. Statistical significance was tested by two sided Fisher's exact test and adjusted for multiple testing using Bonferroni correction.

Fischer *et al.* **Supplementary Figure S7**

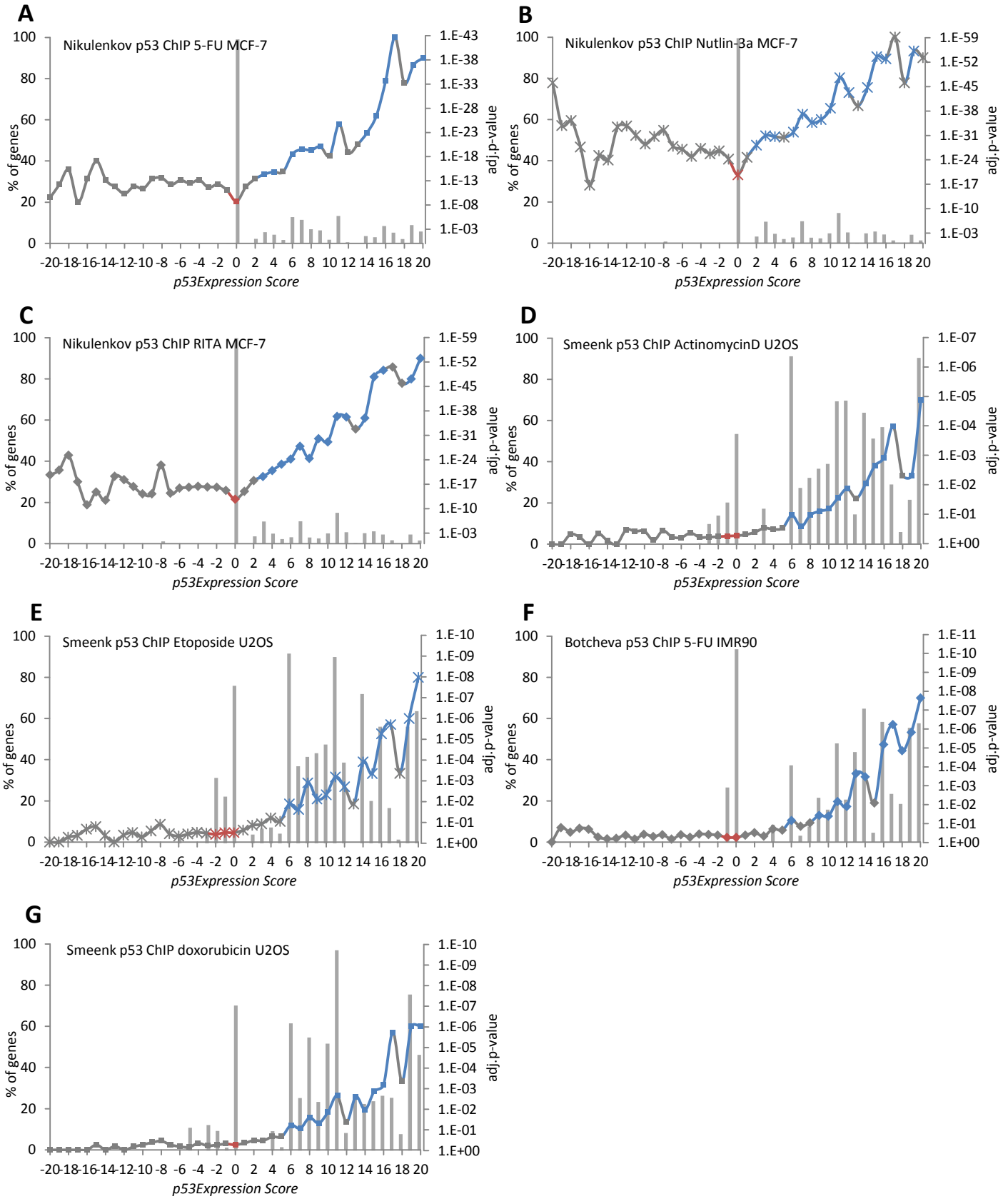

Supplementary Figure S7. TP53 chromatin binding associated with gene activation. The number genes found to be bound by TP53 within ±25 kb from their TSS across the 41 *p53 Expression Score* groups according to the datasets by **(A-C)** Nikulenkov et al., **(D and E)** Smeenk et al. 2011, **(F)** Botcheva et al. and **(G)** Smeenk et al. 2008. Blue and red data points are significantly over- and underrepresented, respectively (adj.p-value ≤ 0.05). Grey data points are not significantly different. Statistical significance was tested by two sided Fisher's exact test and adjusted for multiple testing using Bonferroni correction.

Fischer *et al.* **Supplementary Figure S8**

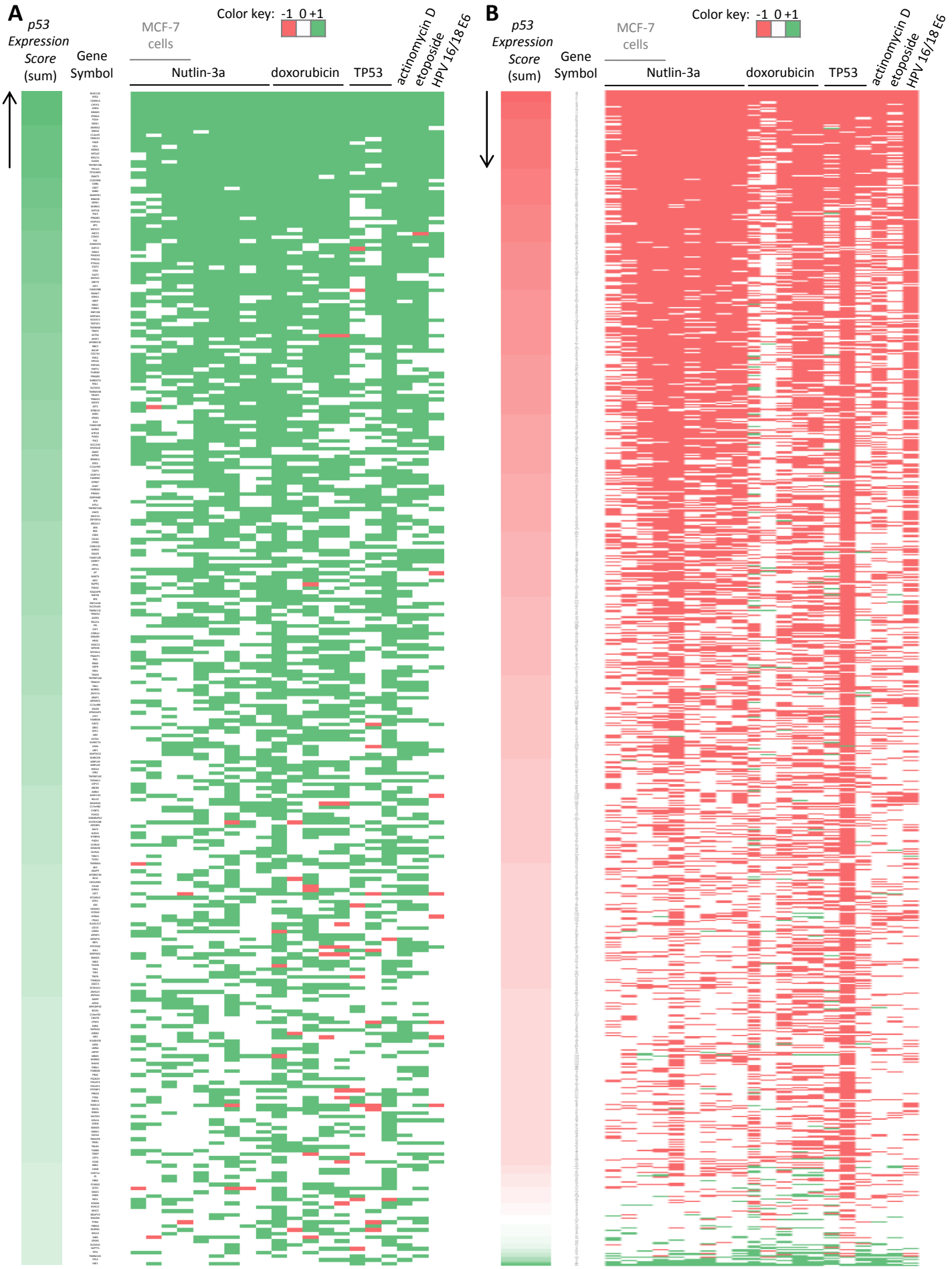

Supplementary Figure S8. Regulation of TP53 and DREAM targets by TP53. A heatmap displaying the regulation of the predicted **(A)** 311 TP53 (Table S3) and **(B)** 971 DREAM target genes (Table S7) across the 20 datasets on TP53-dependent gene regulation.

Fischer *et al.* **Supplementary Figure S9**

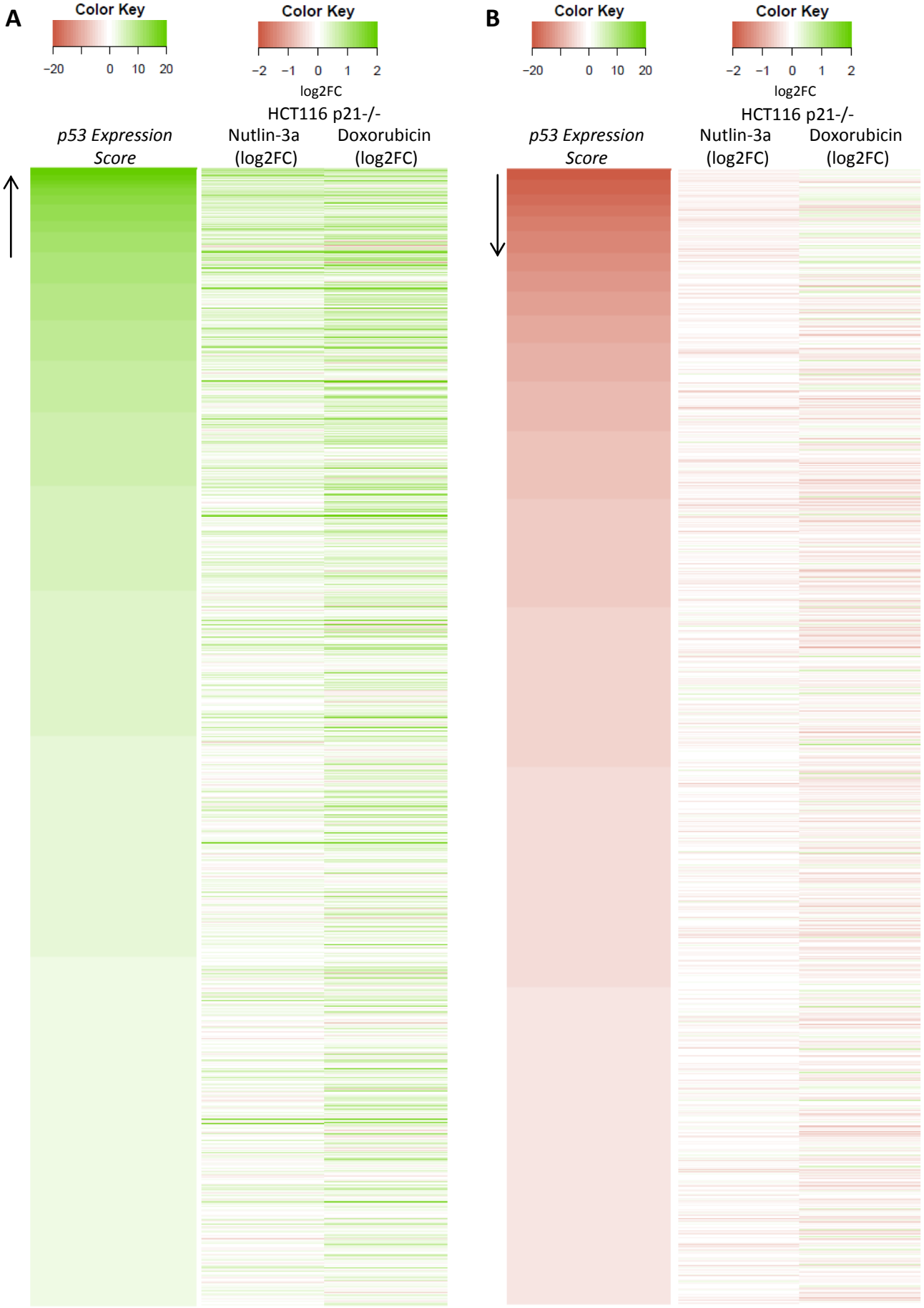

Supplementary Figure S9. Repression by TP53 requires p21. A heatmap displaying the log2(fold change expression) upon Nutlin-3a or doxorubicin treatment in HCT116 p21-/- cells of all genes that have a *p53 Expression Score* **(A)** ≥ 3 and **(B)** ≤ -3.

Fischer *et al.* **Supplementary Figure S10**

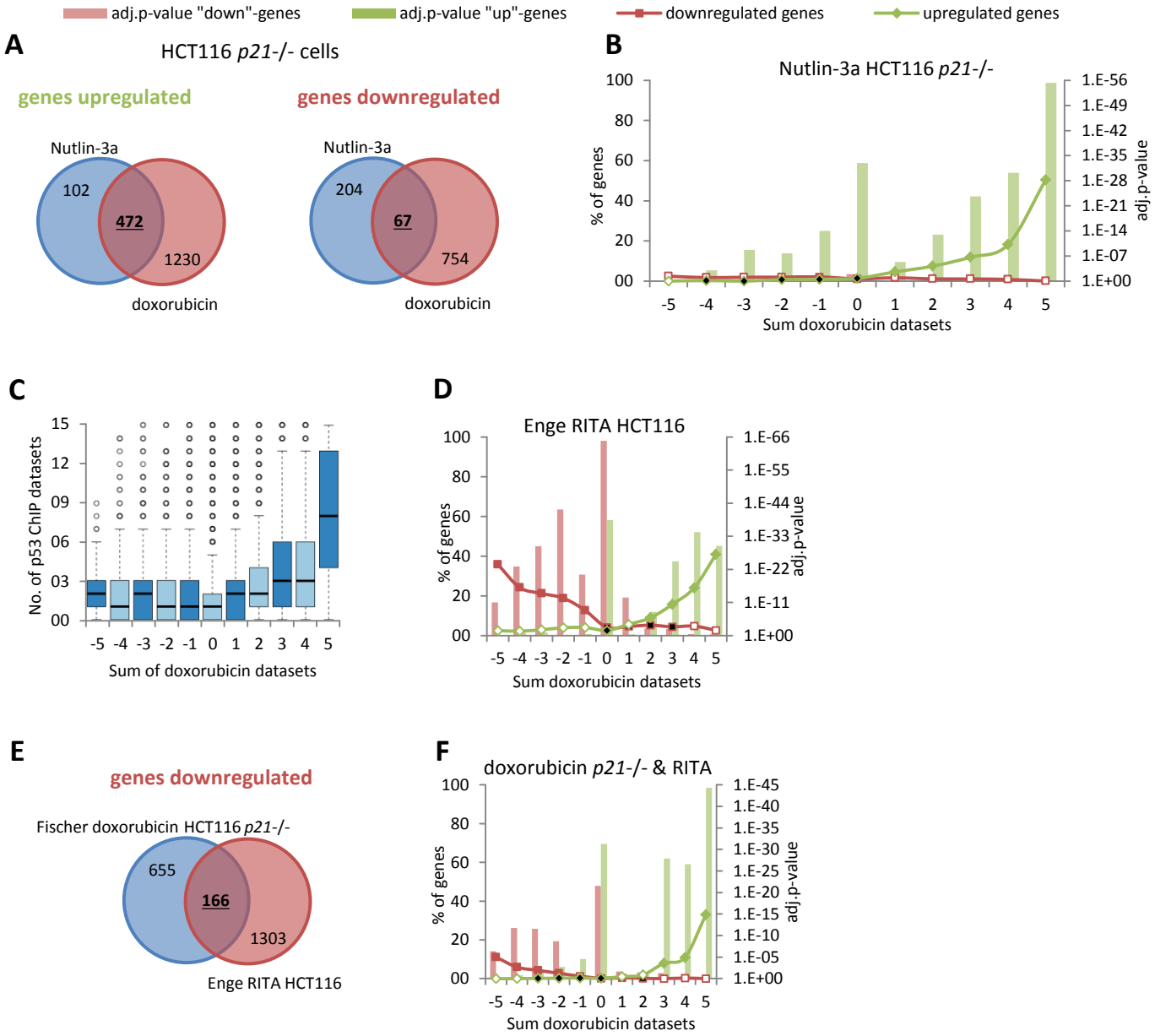

Supplementary Figure S10. The CDK inhibitor p21 is required for TP53-dependent gene downregulation. (A) Venn diagram displaying the overlap of genes that were detected as being TP53-dependently up- or downregulated in the datasets from Nutlin-3a and doxorubicin treated HCT116 *p21*-/- cells. **(B)** The number of genes found differentially regulated in Nutlin-3a treated HCT116 *p21*-/- cells compared to the five doxorubicin datasets. **(C)** Boxplot displaying the number of ChIP datasets that find a gene to be bound by TP53 within ±2.5 kb from their TSS compared to gene regulation from the sum of the five doxorubicin datasets. **(D)** The number of genes detected as as up- or downergulated in Enge et al. is compared to the five doxorubicin datasets. **(E)** Venn diagram displaying the overlap of genes that were detected as being TP53-dependently downregulated by Enge et al. and in the dataset from doxorubicin treated HCT116 *p21*-/- cells. **(F)** The number of genes commonly identified in RITA treated HCT116 cells and doxorubicin treated HCT116 *p21*-/- cells as up- or downergulated is compared to the sum of the five doxorubicin datasets. A two-sided Fisher's exact test was employed to test for significant over- and under-representation of gene sets and p-values were adjusted for multiple testing using Bonferroni correction. Colored and black data points are significantly over- and underrepresented, respectively (adj.p-value ≤ 0.05). White data points are not significantly different.

Fischer *et al.* **Supplementary Figure S11**

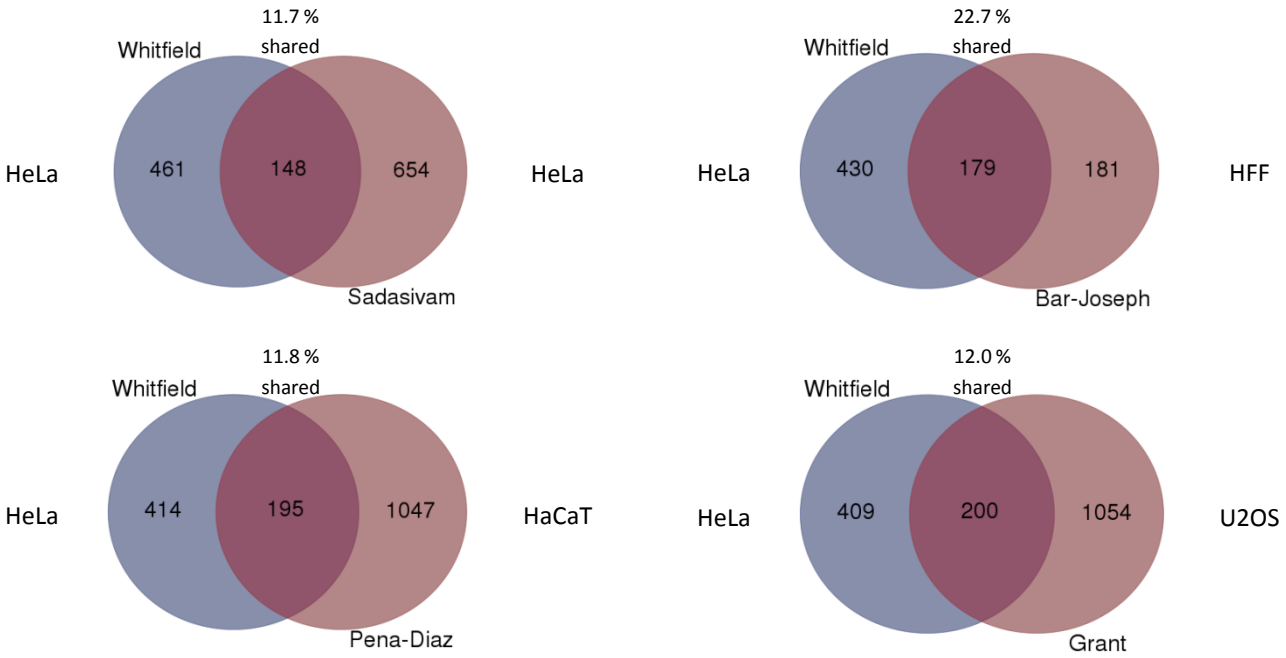

Supplementary Figure S11. Cell cycle-dependent expression profiling studies have small overlaps. Venn diagrams displaying the overlap of genes that were detected as being cell cycle-dependently regulated by Whitfield et al. compared to the genes detected by Sadasivam et al., Bar-Joseph et al., Pena-Diaz et al. and Grant et al.

Fischer *et al.* **Supplementary Figure S12**

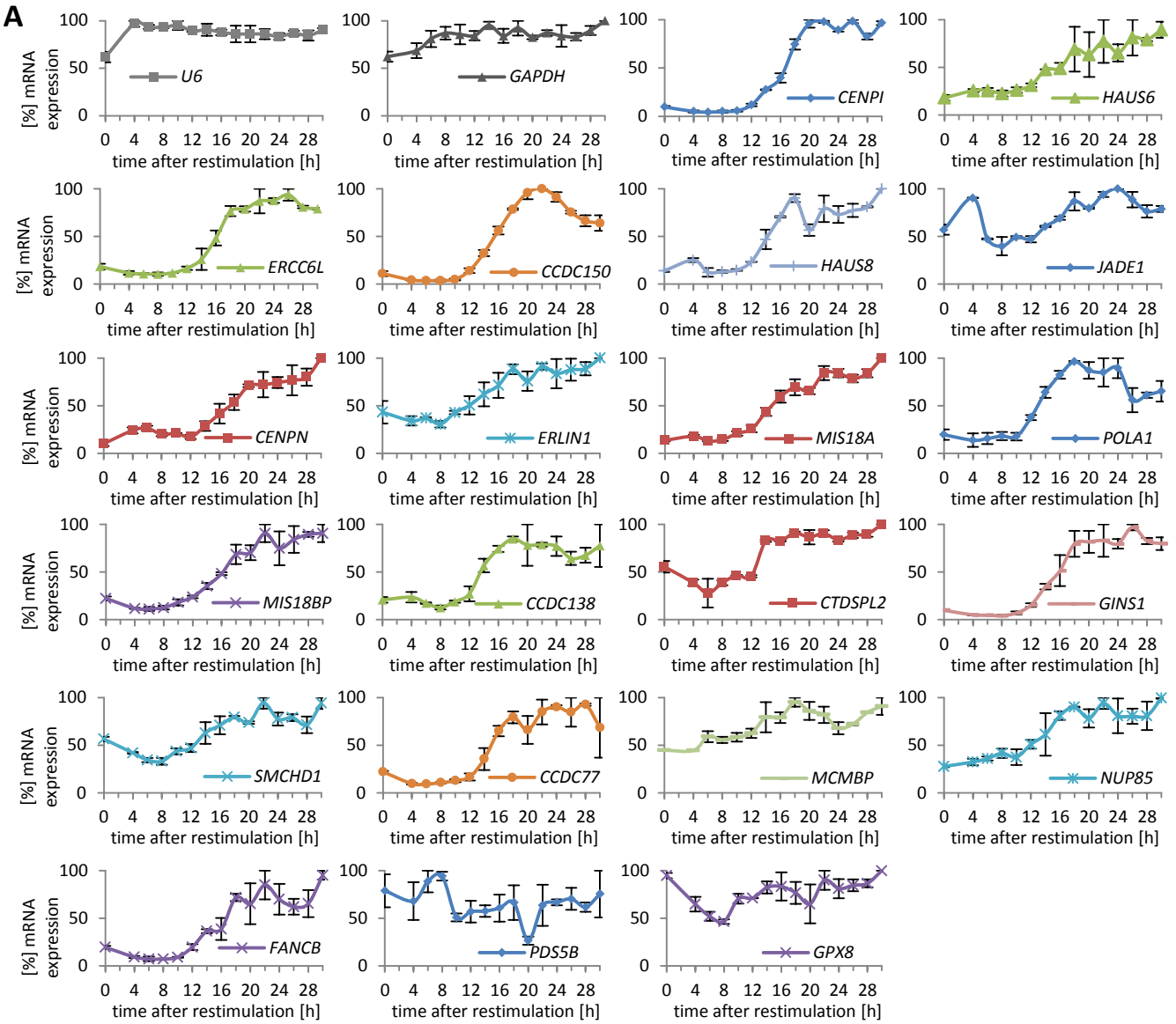

Supplementary Figure S12. TP53-dependent downregulation is highly predictive for cell cycle genes. *CENPI*, *HAUS6*, *ERCC6L* (*p53 Expression Score* -18), *CCDC150* (-17), *HAUS8*, *JADE1* (-16), *CENPN*, *ERLIN1*, *MIS18A*, *POLA1* (-15), *GPX8*, *MIS18BP1* (-14), *CCDC138*, *CTDSPL2*, *GINS1*, *SMCHD1* (-13), *CCDC77*, *MCMBP*, *NUP85* (-12), *PDS5B* (-11) and *FANCB* (-10). **(A)** Expression levels of indicated mRNAs in HFF cells . Experiments were performed in duplicates. Expression of *U6* and *GAPDH* served as negative controls. **(B)** FACS analysis of HFF cells at indicated time points after serum starvation and serum re-addition. Typically, expression increased strongly during the 12 and 14 h time points.

Fischer *et al.* **Supplementary Figure S13**

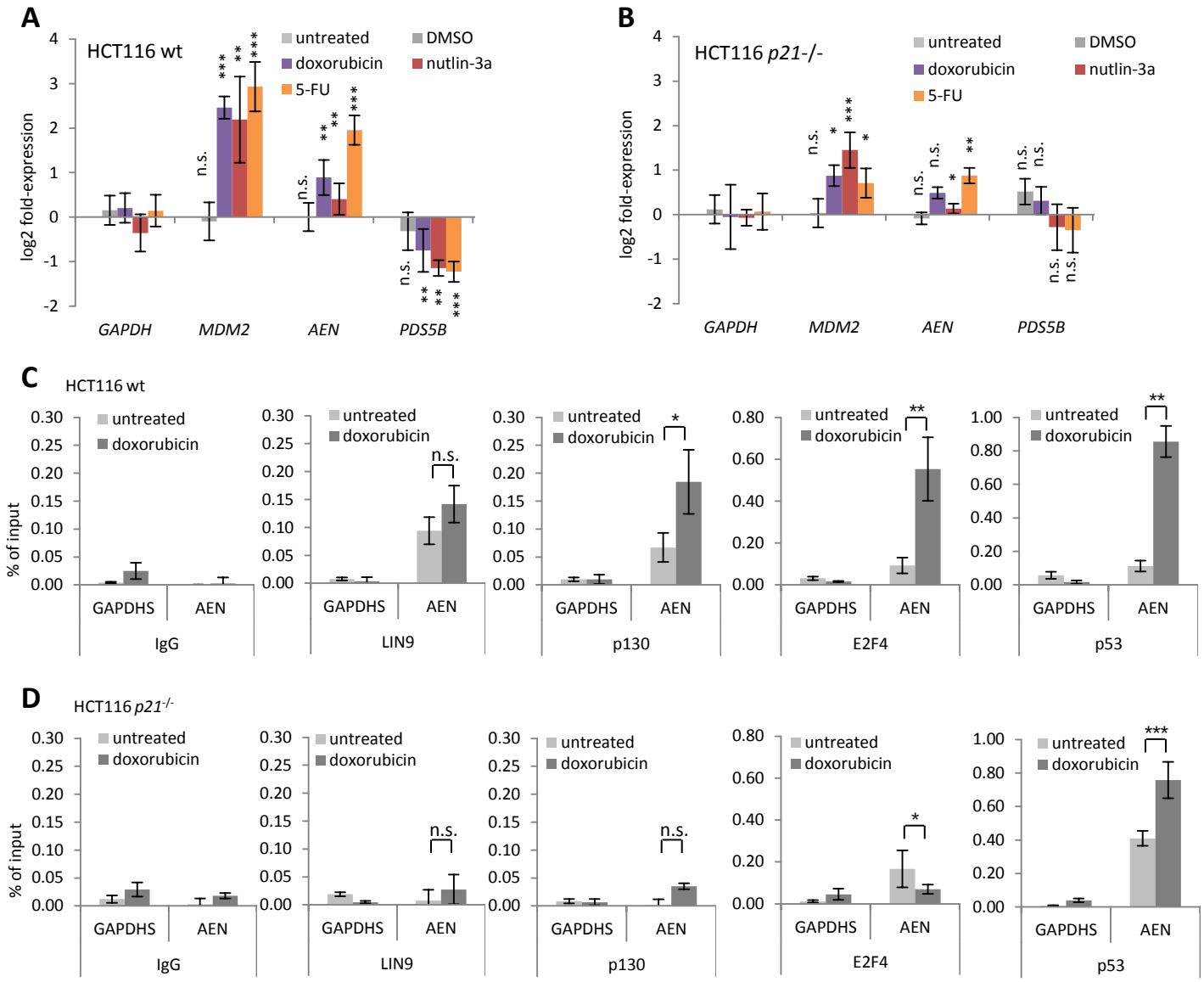

Supplementary Figure S13. *AEN* is a target of DREAM and TP53. The log2-fold change of mRNA expression from treated compared to untreated **(A)** HCT116 wild-type and **(B)** HCT116 *p21*-/- cells is displayed. Cells were treated with doxorubicin, Nutlin-3a, or 5-FU for 24 h. Untreated cells and cells treated with DMSO served as controls. Normalization was carried out against measurements from untreated cells. *GAPDH* expression served as negative control for p53 response, while *MDM2* was employed as positive control. Experiments were performed with two biological replicates and three technical replicates each (n = 6). Protein binding to *AEN* promoter in untreated or 48 h doxorubicin treated HCT116 **(C)** wild-type or **(D)** *p21*-/- cells was tested by ChIP followed by real-time PCR. Protein binding to the *GAPDHS* promoter served as negative control. One representative experiment with three technical replicates (n = 3) is displayed. Significance was tested using the paired Student's t-test; n.s. not significant; *p ≤ 0.05; **p ≤ 0.01; ***p ≤ 0.001.

Fischer *et al.* **Supplementary Figure S14**

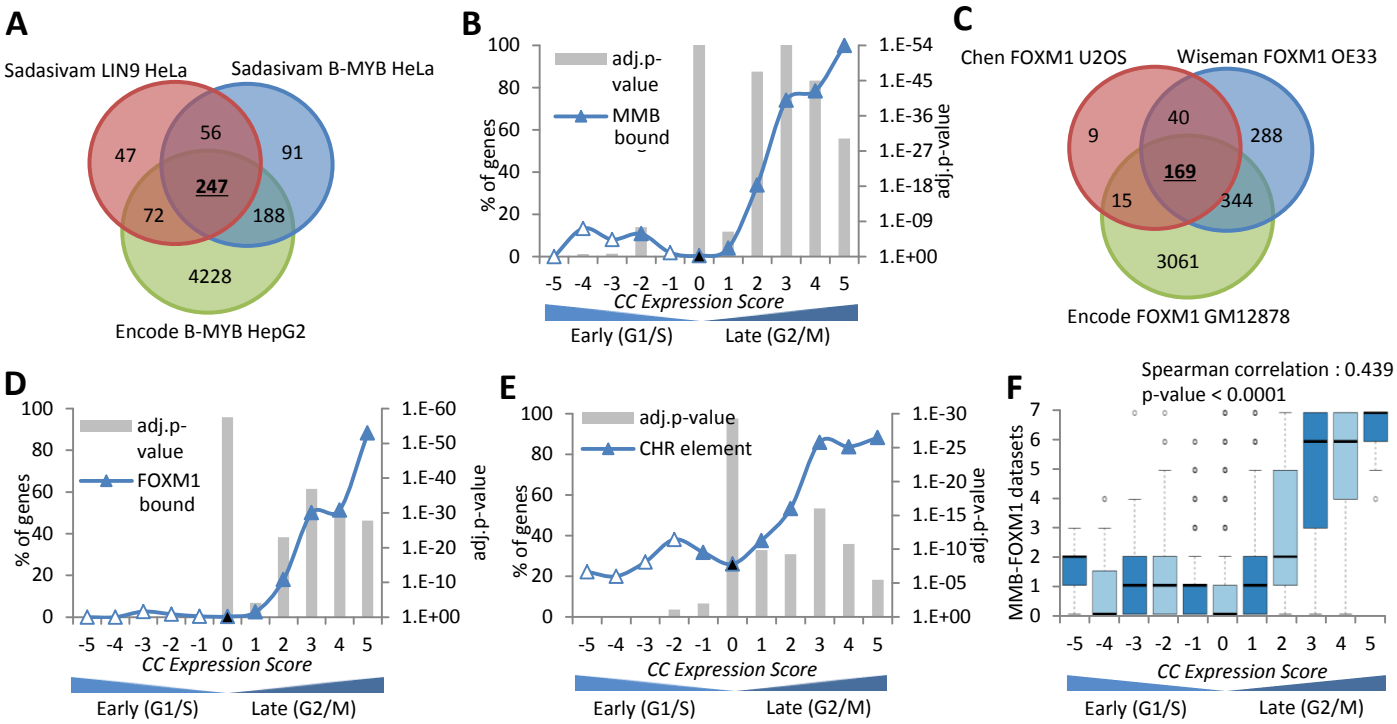

Supplementary Figure S14. MMB and FOXM1 binding to CHR promoter elements identifies G2/M cell cycle genes. Venn diagram of overlaps between genes identified as bound in the ChIP-seq datasets of **(A)** MMB components or **(C)** FOXM1. The number of common **(B)** MMB or **(D)** FOXM1 bound genes or **(E)** genes containing conserved CHR elements across the 11 *CC Expression Score* groups. A two-sided Fisher's exact test was employed to test for significant over- and under-representation of gene sets and p-values were adjusted for multiple testing using Bonferroni correction. Colored and black data points are significantly over- and underrepresented, respectively (adj.p-value ≤ 0.05). White data points are not significantly different. **(F)** Boxplot displaying the sum of these seven MMB-FOXM1 specific datasets across the 11 *CC Expression Score* groups. Correlation coefficient and two-tailed p-value was calculated using GraphPad Prism version 6.00.

Fischer *et al.* **Supplementary Figure S15**

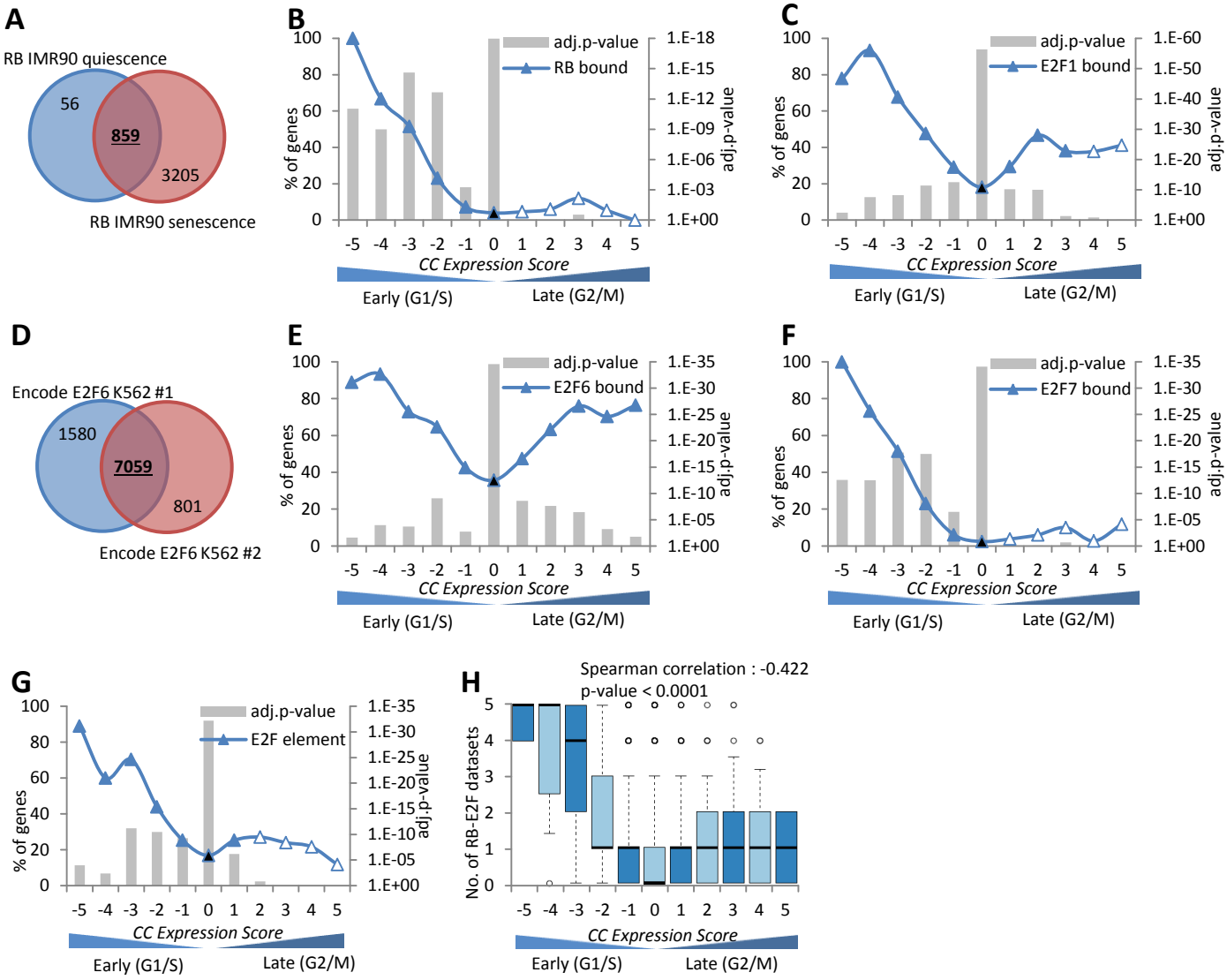

Supplementary Figure S15. RB, E2F1 and E2F7 binding to E2F promoter elements identifies G1/S cell cycle genes. Venn diagram of overlaps between genes identified as bound in the ChIP-seq datasets of **(A)** RB or **(D)** E2F6. The number of common **(B)** RB, **(C)** E2F1, **(E)** E2F6 or **(F)** E2F7 bound genes or **(G)** genes containing a conserved E2F DNA element within their promoter is displayed across the 11 *CC Expression Score* groups. A two-sided Fisher's exact test was employed to test for significant over- and under-representation of gene sets and p-values were adjusted for multiple testing using Bonferroni correction. Colored and black data points are significantly over- and underrepresented, respectively (adj.p-value ≤ 0.05). White data points are not significantly different. **(H)** Boxplot displaying the sum of the five RB-E2F specific datasets across the 11 *CC Expression Score* groups. Correlation coefficient and two-tailed p-value was calculated using GraphPad Prism version 6.00.

Fischer *et al.* **Supplementary Figure S16**

A

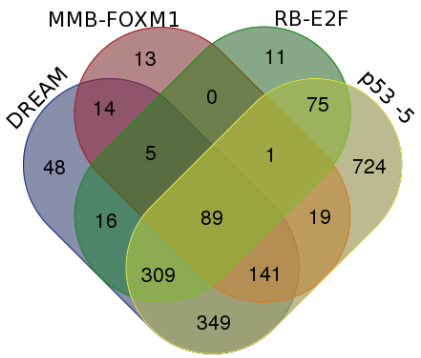

B

Term	FDR
ncRNA metabolic process	1.37E-05
ncRNA processing	5.94E-04
cellular amino acid biosynthetic process	8.53E-04
rRNA metabolic process	1.71E-03
ribonucleoprotein complex biogenesis	4.20E-03
rRNA processing	4.95E-03
ribosome biogenesis	1.01E-02
RNA processing	2.17E-02
amine biosynthetic process	2.71E-02

Supplementary Figure S16. Genes down-regulated by TP53 are primarily targets of DREAM, RB-E2F and MMB-FOXM1. (A) Venn diagram of overlaps between genes predicted as DREAM, MMB-FOXM1, or RB-E2F target and genes that have a *p53 Expression Score* ≤ -5. **(B)** BP GO terms with their FDR value as identified using the DAVID Functional Annotation Tool enriched among the 724 genes that have a *p53 Expression Score* ≤ -5 but are no potential DREAM, RB-E2F, or MMB-FOXM1 targets.